A Coarse-Grained Model of Poly(phenylene-sulfide) via Multi State Iterative Boltzmann Inversion

Chris Jones, Marjan Albooyeh, Eric Jankowski

E-mail:

Introduction

Poly(phenylene sulfide) (PPS) is a semi-crystalline, high-performance thermoplastic polymer used across a broad spectrum of applications spanning several industries.[1–3] For example, PPS is used as an insulating thin film in capacitors that demand high-temperature performance,[4] as an abrasion and chemical resistant coating,[5?] and can be made conductive via doping for use in organic electronics.[2,6,7] Additionally, PPS is emerging as a popular choice as the matrix material in high-performance thermoplastic composites where its superior mechanical strength, chemical resistance, and relatively low processing temperature are ideal properties for high-throughput manufacturing of next-generation aerospace composites.[8–10] As a widely adopted polymer with diverse industrial and manufacturing applications, developing computational models of PPS that offer unique mechanistic insights into the relationships among its structure, processing, and properties is crucial for advancing engineering practices and optimizing manufacturing processes of PPS. The current body of work for computational modeling of PPS appears to mostly consist of all-atom molecular dynamics (MD) models that focus on injection molding,[11–13] adhesion of PPS with a single-wall carbon nanotube[14] and disintegration under extreme temperatures using reactive MD.[15] However, polymer engineering and material science questions often require a multiscale modeling approach in order to capture the length scales of polymer microstructures and time scales of polymer relaxation and diffusion processes.[16–18] Coarse-grained (CG) MD is one approach commonly used in multiscale modeling of polymers that is able to access large time and length scales more efficiently than atomistic simulations, while still providing the mechanistic insight of particle-based simulation methods.[18,19] A CG model consists of choosing a lower-resolution structural representation of the underlying material by grouping chemical moieties into single "super atoms", or beads, and deriving their effective interaction potentials. Several approaches exist for deriving CG potentials, each tailored to optimize distinct elements of the underlying physics and material properties of the system being studied.[20,21] Broadly, these approaches include top-down methods, where CG models are tuned to reproduce specific macroscopic material properties, and bottom-up methods, which derive CG models from quantum mechanical principles or use target data from atomistic molecular dynamics simulations to capture fine-scale interactions. Various data-driven approaches to bottom-up modeling include structure matching, force matching, and relative entropy minimization, each offering unique advantages in reproducing the atomistic behavior of polymer systems. Structure matching excels at capturing equilibrium structure like radial distribution functions and intra-molecular distributions of bond lengths, angles and dihedrals.[22–24] Force matching, on the other hand, seeks to reproduce forces from atomistic simulations, making it particularly effective at producing equivalent trajectories of the underlying model.[25,26] Relative entropy minimization optimizes the entire distribution of configurations, balancing accuracy across a broad range of thermodynamic and structural properties.[27,28] Iterative Boltzmann inversion (IBI) is a commonly used structure-matching approach for creating CG models of polymers, and is designed to derive CG potentials by matching bonded and non-bonded distributions from a target fine-grain model.[22,23,29–32] Multistate iterative Boltzmann inversion (MSIBI), developed by Moore *et al.*, expands upon IBI by including target distributions from multiple state points when deriving a single CG potential, which has been shown to improve the phase-space transferability of the CG potential.[24,33–36] In this work, we take a structure matching approach with the application MSIBI to develop a coarse-grain model of PPS, and to the best of the author's knowledge, this work represents the first reported coarse-grained model of PPS polymers.

Methods

Atomistic Model

In order to create target trajectories for deriving CG potentials of both intra-molecular and inter-molecular interactions, we run simulations of two different kinds of systems: 1) single chain, low density, simulations used to obtain target intra-molecular distributions of bond lengths, angles, and dihedrals, and 2) bulk simulations used to obtain target non-bonded pair-wise distributions. The single chain systems have 40 repeat units and run at a density of $0.0001\frac{g}{cm^3}$ (i.e. a vacuum). The bulk systems consist of 50 polymer chains with 20 repeat units each.

We use the `flowermd` python package to build molecules of PPS polymers, create initial configurations and run both target and coarse-grained simulations.[37] MD simulations use the HOOMD-Blue simulation engine[38] and run on NVIDIA P100 GPUs. We use the python package `signac`[39] to manage simulations workflows and data analysis on the `Fry` super computer cluster located at Boise State University. All target simulations employ the 12-6 Lennard Jones pair potential as shown in Equation 1,[40] harmonic potentials for bond stretching and bending as shown in Equation 2 and Equation 3 respectively, and the OPLS style dihedral potential as shown in Equation 4.[41] The pair interactions exclude 1-2 and 1-3 pairs and utilize a 1-4 pair scaling of 0.5.

$$V_{LJ}(r) = 4\epsilon\left[\left(\frac{\sigma}{r}\right)^{12} - \left(\frac{\sigma}{r}\right)^{6}\right] \tag{1}$$

$$V_{bond}(l) = \frac{1}{2}k\left(l - l_0\right)^2 \tag{2}$$

$$V_{angle}(\theta) = \frac{1}{2}k\left(\theta - \theta_0\right)^2 \tag{3}$$

$$V_{torsion}(\phi) = \frac{1}{2}k(1 + d\cos\left(n\phi - \phi_0\right)) \tag{4}$$

Throughout this work, unless otherwise indicated, we report distances in units of coarse-grained simulation element diameters (σ), and energy (ϵ) in units of the strongest non-bonded interaction of the underlying UA model, and their values are $\sigma = 0.3438$ nm and $\epsilon = 1.065$ kJ/mol. Simulation scripts we use in the work described here, an `xml` file with atomistic force field parameters usable with `flowerMD`[37] and `foyer`,[42] and the final coarse-grain potential files are all available at `https://github.com/chrisjonesBSU/pps-msibi`.

Initial configurations of the bulk systems are built by packing a low density box with PPS polymer chains and performing a temperature and volume annealing simulation to reach a starting density of $1.35\frac{g}{cm^3}$ over a period of 2×10^7 time steps while annealing from a relatively high reduced temperature of $kT = 6.0$ to the set state point temperature with a step size of $dt = 0.0003$. After shrinking, a short NVT simulation is performed for 1×10^7 time steps before equilibrating in the NPT ensemble at atmospheric pressure. From the NPT simulations, equilibrium volumes are sampled at each state point, and we run a short box update to the average equilibrium volume before finally equilibrating in the NVT ensemble. We run simulations of the bulk configurations over a reduced temperature range of $kT = 2.0$ to $kT = 4.6$. Equilibration times varied for each state point, so we do not report on the number of time steps used to achieve equilibration, instead we identify trajectory equilibration and perform subsequent sampling using the time series module of the `pymbar` python package.[43,44]

Atomistic Model Validation

In order to ensure the data used in deriving a coarse model of PPS is faithfully capturing the material properties of PPS, we validate the model described above by measuring T_g, crystallization temperatures, and densities. A commonly used method in MD to measure T_g is to perform a series of NPT ensemble simulations over a temperature range and measuring the density, or specific volume (v), as a function of temperature where the inflection point of the slope $\frac{dv}{dT}$ indicates T_g.[45,46] This approach works well when the slopes are smooth and continuous before and after the inflection point; however, when the conditions are such that the polymer system begins to relax to semi-crystalline morphologies, sudden increases in the density will occur. In this work, we also use an alternative method to find T_g which measures monomer self-diffusion coefficients ($\mathcal{D}_{self}$) over temperatures ranging from below to above T_g, and the temperature where $\mathcal{D}_{self}$ departs from 0 indicates T_g.[47] Henry *et al* show this method accurately measures T_g in thermoset polymer systems.[48] We use the nematic order parameter, often referred to as the $S2$ order parameter, to measure orientational ordering of polymer chains in bulk systems. We use $S2$ and radial distribution functions (RDF) as a description of crystallinity (i.e. containing both positional and orientational order) to identify crystallization temperatures of PPS, which is the temperature range above T_g where crystallization kinetics occur most rapidly upon heating.[49] We use the `freud` python package for calculating $S2$, RDFs, and mean-square displacements (MSD) used in finding $\mathcal{D}_{self}$.[50] $S2$, RDFs and MSDs of U.A. systems are calculated with the coarse-grain mapping scheme applied as shown in Figure 1, and the vectors used in $S2$ calculations are the set of monomer-monomer bond vectors.

Coarse Graining

We use a simple mapping scheme that maps one PPS monomer to one bead as shown in Figure 1. With this mapping scheme, the final coarse-grain model will contain a bond potential $V_{A-A}(l)$, angle potential $V_{A-A-A}(\theta)$, pair potential $V_{A,A}(r)$ and dihedral potential

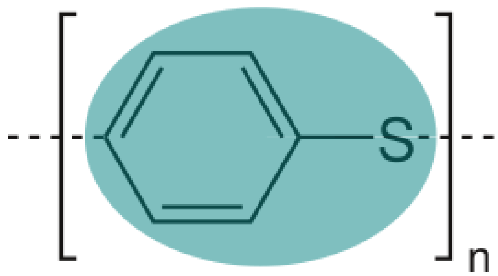

Figure 1: Coarse-grain mapping of 1 bead per PPS monomer.

$V_{A-A-A-A}(\phi)$ where the coarse-grained beads are labelled as A. Structure-matching methods such as IBI and MSIBI typically optimize one interaction type at a time in the order of their relative strength, which follows as:[22,23]

$$V_{stretching} \rightarrow V_{bending} \rightarrow V_{pair} \rightarrow V_{dihedral}$$

Following this order, we set the optimized coarse-grained potential from the previous interaction when optimizing the next. For example, when optimizing the bond bending potential, the bond stretching potential is included, but pair interactions are not accounted for, and when optimizing the pair potential, the previously obtained bond stretching and bending potentials are included and held static. In this work, bond lengths and bond dihedrals both yield simple distributions where we take the Boltzmann inverse following

$$V(x) = -k_b T \ln\left[P(x)\right], \tag{5}$$

from which we fit to the functional forms given by Equation 2 for bond stretching and Equation 4 for bond dihedrals.

The distributions for bond angles and non-bonded pairs are not as simple or well suited to fitting functional forms, so each interaction is optimized using MSIBI where an initial "guess" potential is set for the first iteration and after each iteration the resulting structural distributions are compared against the target distributions, and the coarse-grained potential is updated according to:

$$V_{i+1}(x) = V_i(x) - \frac{1}{N}\sum_s \alpha_s k_B T_s \ln\left[\frac{P_s^i(x)}{P_s^*(x)}\right], \tag{6}$$

where N represents the number of state points, k_B is the Boltzmann constant, T_s denotes the temperature of the state point, and $P_s(x)$ is the structural distribution associated with the potential $V(x)$ of state s. The target distribution is denoted as $P_s^*(x)$. The parameter α serves a dual role: firstly, as a damping factor, or learning rate, limiting the potential update magnitude of each iteration, and secondly, as a state-point weighting factor.[24] Therefore, each state can be assigned a distinct value of α, determining its influence on the final potential. As $P_s(x)$ approaches $P_s^*(x)$, the right side of the equation approaches zero, at which point $V_{i+1}(x) \equiv V_i(x)$, and further iterations are not necessary.

In our experience, effort spent getting as close as possible with the initial guess potential is not needed. It is only necessary that the initial potential yields a distribution that shares some region of overlap with the target distribution, even if the shape and magnitude of the distributions are initially quite different. As a result, for optimizing angles, we begin with a harmonic angle potential (Equation 3) with $\Theta_0 = 2.9$ radians and $k = 300\epsilon$, and pairs use an initial guess of a 12-6 Lennard-Jones potential (Equation 1) with $\sigma = 1.5$ and $\epsilon = 1.0$. The set of state points used in deriving CG pair potentials are given in Table 1 and were selected so that they covered the temperature range from below T_g to above T_m, and the densities are the result of their corresponding NPT simulations.

Table 1: State points values of temperature and density used in deriving CG pair potentials with MSIBI.

State	**Density (g/cm^3)**	**Temperature (C°)**
A	1.32	80
B	1.17	150
C	0.74	300

Coarse-grain Model Validation

The coarse-grained potential performance in re-creating target distributions is reported as f_{fit} and is measured by the curve-fitting score

$$f_{fit} = 1 - \frac{\sum_{x_{start}}^{x_{cut}} (|P^i(x) - P^*(x)|)}{\sum_{x_{start}}^{x_{cut}} (|P^i(x)| + |P^*(x)|)} \tag{7}$$

where $P^i(x)$ is the distribution obtained from iteration i of the coarse-grain model and $P^*(x)$ is the target distribution.[24] In the case of a perfect match between CG and target distributions, the numerator of the second term goes to zero, and $f_{fit} = 1.0$.

We further evaluate the CG model performance by comparing commonly used statistical measurements of polymer structure such as the radius of gyration (R_g), end-to-end distance (R_e) and persistence length (ℓ_p) between the UA and CG models of single chain simulations over chain lengths ranging from $N = 20$ to $N = 80$ repeat units. R_g measurements are performed using `freud`[50] and ℓ_p values are calculated with `MDAnalysis`.[51,52]

Results

Atomistic Model

Measured densities and $S2$ order parameters over the temperature range studied are shown in Figure 2. Reported values for PPS densities range from 1.35 $\frac{g}{cm^3}$ for semi crystalline to a crystallographic density of 1.44 $\frac{g}{cm^3}$ reported by Tabor *et al.*[53] and 1.42 $\frac{g}{cm^3}$ by Lovinger *et al.*[54] $S2$ is an order parameter that describes orientational order, ranging from $S2 = 0$ (no orientational ordering) to $S2 = 1$ (perfect orientational ordering), and can be used as a description for crystallization in polymer morphologies where the lamellar structure formed by chains folding back on to themselves give rise to nematic ordering of chain backbones.[55,56] At T_g, we see both a sharp increase in density (Figure 2 (a)) and the onset of increased orientational ordering (Figure 2 (b)). More specifically, within reported experimental values of cold crystallization temperatures (T_c) of PPS,[57?] we see densities approaching crystalline density, reaching a density of $1.40\frac{g}{cm^3}$, and a significant increase in orientational ordering which then steadily decreases as temperatures approach T_m. The RDF of the state point with the largest $S2$ value is shown in Figure 2 (d) where the first two peaks occur at distances of $0.561\,nm$ and $0.861\,nm$ which are in great agreement with reported lattice parameters of $0.561\,nm$ and $0.867\,nm$.[53,54] Also, in Figure 2(b), the onset of chain mobility corresponds with T_g where we see values for $\mathcal{D}_{self}$ begin to steadily increase from $\mathcal{D}_{self} = 0\frac{m^2}{s}$ at a temperature of $86°C$.

Coarse Grain Model

Parameters obtained fitting to the Boltzmann inverse (Equation 5) for harmonic bonds (Equation 2) yield $k = 1777.6\epsilon$ and $l_0 = 1.4226\sigma$ and for periodic dihedrals (Equation 4) give $k = 8.0\epsilon$, $\phi_0 = 0$ radians, $d = -1$ and $n = 1$. The final angle and pair potentials we obtain from MSIBI, are shown in Figure 4. The angle potential resembles a torsion-like energy landscape with trans and gauche states separated by an energy barrier, which implies that the angular degrees of freedom in the CG model are capturing the effect of backbone monomer torsional states of the atomistic model.[58] The energy constant of $k = 8.0\epsilon$ in the dihedral term is relatively weak compared to the other components of the complete forcefield. Removing the dihedral force from the CG model has no effect on matching bulk structure, bond length and angle distributions, but does result in slightly poorer performance in matching statistical chain measurements such as R_e, R_g, and more notably ℓ_p as is shown in **??**.

The CG model's performance in matching intramolecular distributions of bond lengths, bond angles, and bond dihedrals is shown in Figure 4 with good agreement for each with f_{fit} values (Equation 7) of 0.992, 0.977, and 0.975 respectively. The match and f_{fit} values between target and C.G. RDFs of each state used in MSIBI are shown in Figure 5 where we also see good agreement across all three states.

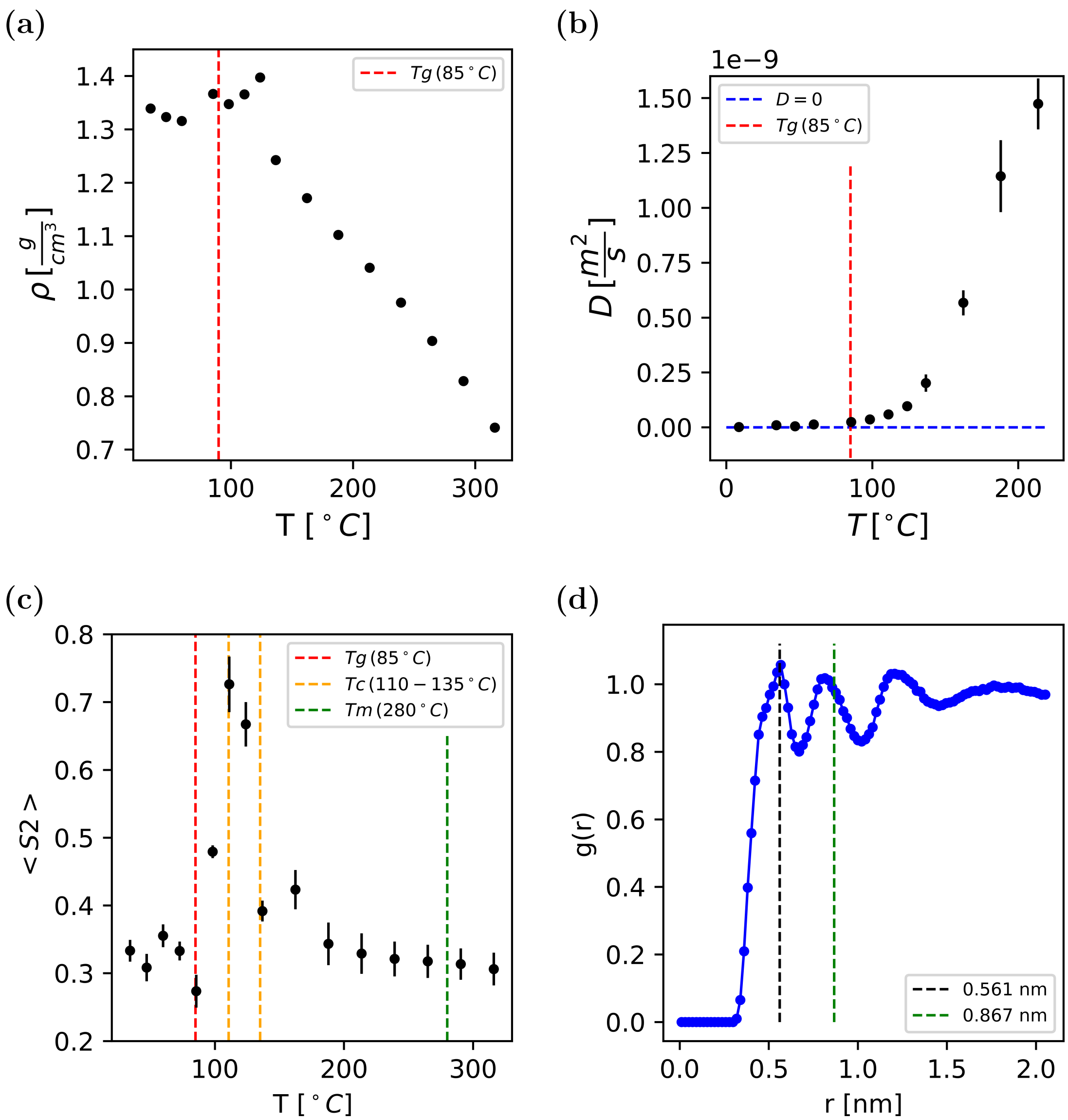

Figure 2: Measured densities (a), self-diffusion coefficients (b), nematic order parameters (c) over the simulated temperature range studied, and the RDF corresponding to the temperature with the largest nematic ordering (d) with reported crystalline lattice constants shown by the dashed lines.

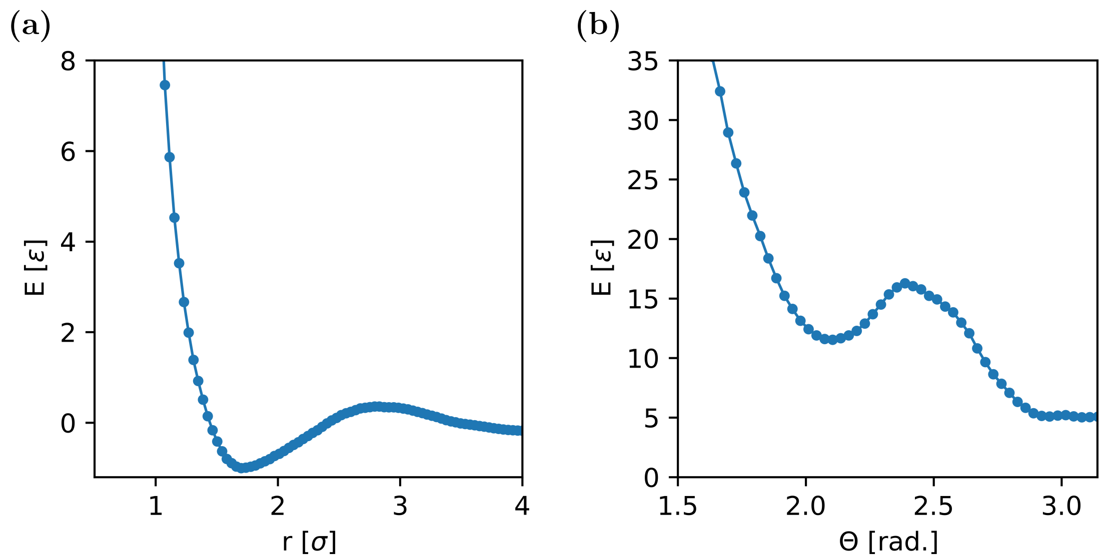

Figure 3: Final potentials obtained from MSIBI for pairs (a) and angles (b).

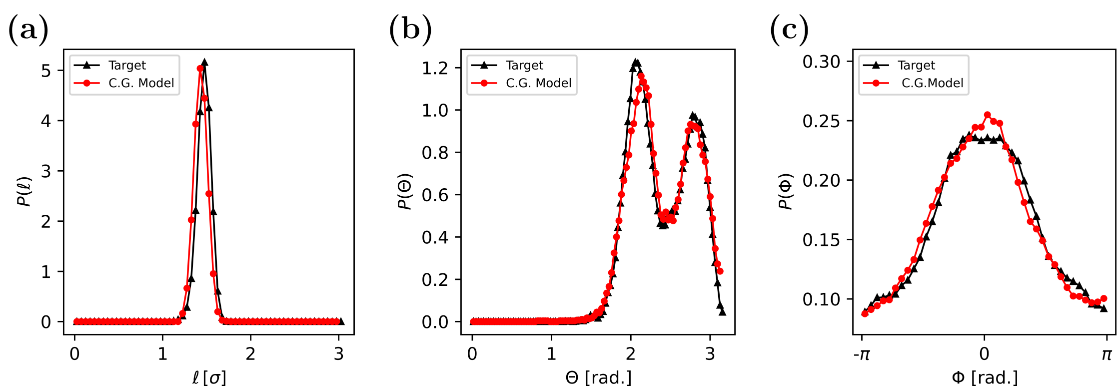

Figure 4: Intramolecular distribution matching of the coarse-grain model for bonds (a), angles (b) and dihedrals (c).

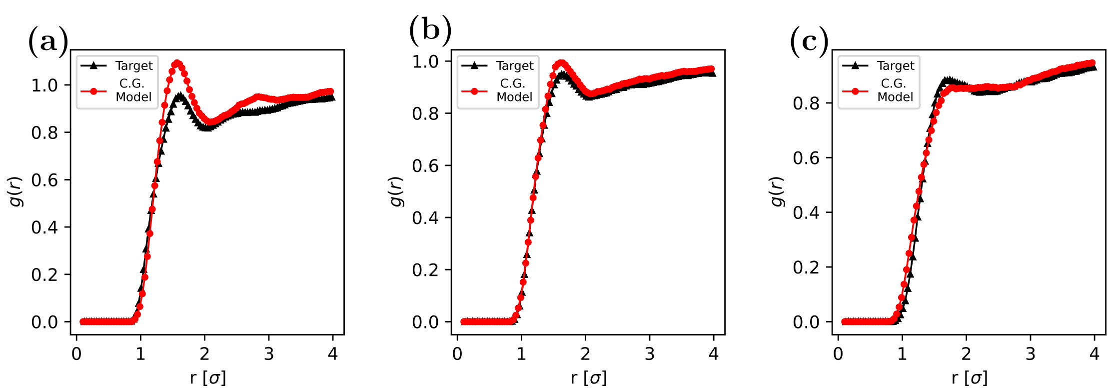

Figure 5: Pair-wise distribution matching of the coarse-grain model for state A ($f_{fit} = 0.971$) (a), state B ($f_{fit} = 0.988$) (b), and state C ($f_{fit} = 0.986$) (c).

The IBI, and MSIBI, methods are designed so that CG potentials are derived from matching structural distributions, so results of good agreement across structural distributions are not necessarily surprising. To further test the overall performance of the CG model, we compare commonly used polymer statistical measurements of end-to-end distance (R_e), radius of gyration (R_g) and persistence length (ℓ_p) between the target and CG models in Figure 6.

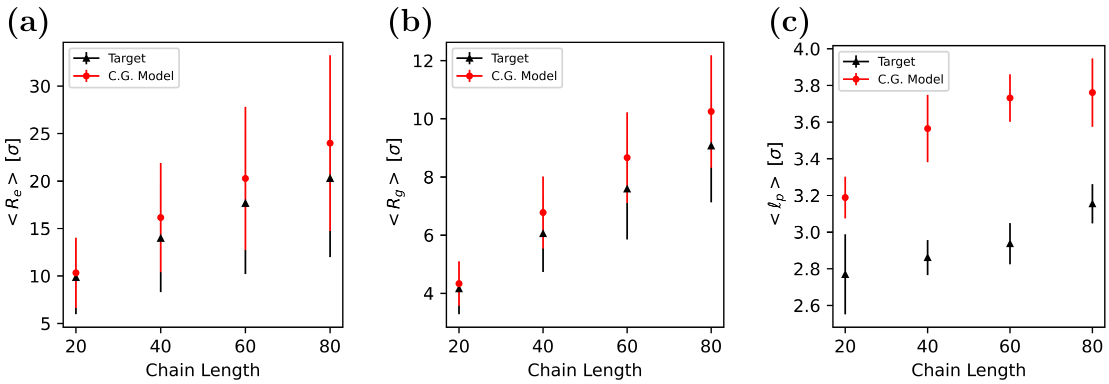

Figure 6: End-to-end distance (a), radius of gyration (b) and persistence length (c) comparison between target and C.G. models.

The performance of the coarse-grain model's time steps per second (TPS), and how it scales with the number of monomers is shown in Figure 7. These TPS results are obtained from simulations running on NVIDIA P100 graphics processing units with 16GB of VRAM using the Hoomd-Blue simulation engine.[38] The largest system tested contains 288,000 coarse-grain beads, equivalent to 2,016,000 beads in the U.A. model, and achieved an average TPS of just over 500. U.A. models of the same systems in Figure 7 are not simulated due to computational limitations, but for comparison, the U.A. systems described in Section **Atomistic Model** contains 1,250 monomers and achieved an average TPS on the order of 1,000, while the same size system of the C.G. model reaches TPS values around 10,000.

Discussion

Despite the popularity of PPS across many industries, particle-based computational modeling of PPS to predict structure-property relationships appears to be relatively sparse,

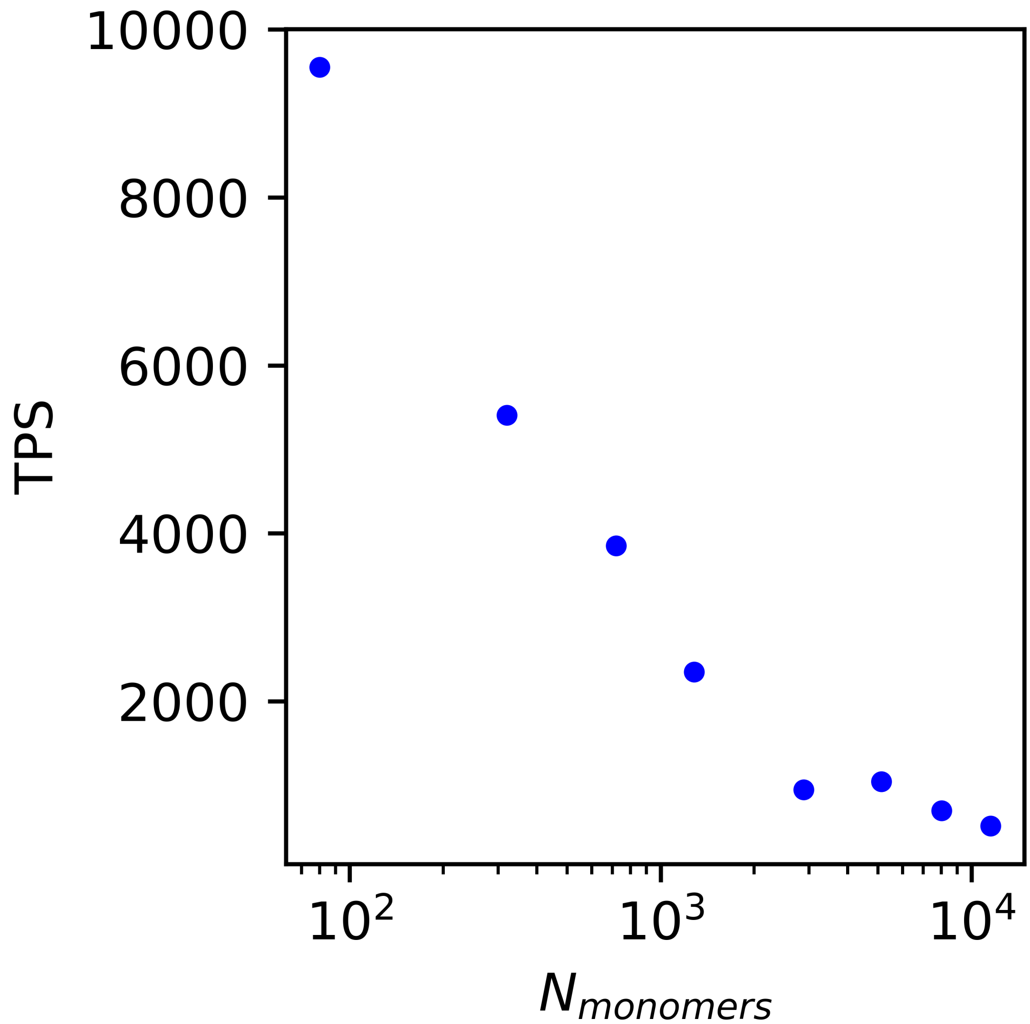

Figure 7: TPS performance of the C.G model over a range of system sizes.

especially in utilizing multiscale modeling methods such as coarse grained molecular dynamics. The united-atom model presented here is able to successfully capture several important characteristics of PPS, including glass transition, crystallization kinetics and semi-crystalline structure observed experimentally. The CG model developed accurately replicates amorphous PPS structure across temperatures ranging from below T_g to above T_m, matches intramolecular distributions, and successfully reproduces polymer chain structural parameters (R_e, R_g, ℓ_p) which directly affect several bulk properties of polymers.[?] However, challenges still remain in developing a complete CG model of PPS. It is worth highlighting that the three state points chosen (Table 1) do not include any of the semi-crystalline state points that exhibit both high orientational and spatial ordering (Figure 2 (c) and (d)). This isn't necessarily by choice as the crystalline phase of PPS is important to multiscale modeling efforts, but preliminary work proved difficult to produce pair potentials that could fit both amorphous and crystalline state points simultaneously. This is indicative of a possible limitation of CG potentials of semicrystalline polymers that utilize isotropic (i.e. spherical) pair potentials–as is the case in IBI and MSIBI. This is especially true for simple linear polymers such as PPS that don't contain side groups that can give rise to crystalline structure, for example, as has been shown in isotropic CG models of P3HT.[59–61] Previously developed isotropic CG models of linear polymers polyvinyl alcohol[62] and polyethylene[58] show a tendency to form crystalline lamellar structures driven by the CG angle potentials which in both cases contain trans and gauche states, similar to the angle potential in this work (Figure 3 (b)). However, these do not recreate their experimental orthorhombic crystalline structures, which PPS also shows experimentally.[53,54]

Perhaps, a more thorough CG model of PPS requires anisotropic pair potentials, such as the Gay-Berene (GB) potential[63] where forces are calculated as a function of distance and orientation which therefore effectively takes into account the non-spherical shape of the underlying molecules being coarse-grained. While much effort has been spent creating CG models that utilize a GB pair potential for small organic molecules and oligomers,[61,64–67] approachable and robust methods for deriving chemically specific GB parameters for CG polymer models are not well established.[21] Additionally, machine learning approaches to developing CG models of polymers are growing in popularity[68–72] and are a promising solution to the challenge of developing anisotropic CG models for organic molecules.[68,73] However, this approach also suffers from a lack of established and transferrable methods. Furthermore, obstacles remain in the implementation of machine learned models into existing simulation engines where, for example, the use of neural-network potentials may not necessarily result in increased computational efficiency desired by using CG models despite the reduced degrees of freedom achieved by coarse-graining.[74,75]

Here, MSIBI is chosen as the coarse-graining method because of its straight forward implementation, interpretability, and because the resulting potentials (i.e. fitting to free parameters and table potentials) provide immediate compatibility and significant performance improvement with established simulation engines, all of which are needed to effectively begin multiscale modeling of PPS.

Conclusion

References

(1) Zuo, P.; Tcharkhtchi, A.; Shirinbayan, M.; Fitoussi, J.; Bakir, F. Overall Investigation of Poly (Phenylene Sulfide) from Synthesis and Process to Applications—A Review. *Macromolecular Materials and Engineering* **2019**, *304*, 1–27.

(2) Rahate, A. S.; Nemade, K. R.; Waghuley, S. A. Polyphenylene sulfide (PPS): State of the art and applications. *Reviews in Chemical Engineering* **2013**, *29*, 471–489.

(3) Furushima, Y.; Nakada, M.; Yoshida, Y.; Okada, K. Crystallization/Melting Kinetics and Morphological Analysis of Polyphenylene Sulfide. *Macromolecular Chemistry and Physics* **2018**, *219*, 1–7.

(4) Ho, J.; Jow, R. Characterization of High Temperature Polymer Thin Films for Power Conditioning Capacitors.

(5) Sugama, T.; Webster, R.; Reams, W.; Gawlik, K. High-performance polymer coatings for carbon steel heat exchanger tubes in geothermal environments.

(6) Takai, Y.; Inoue, M.; Shibata, A.; Mizutani, T.; Ieda, M. Electrical Properties of High-Molecular-Weight Poly-P-Phenylene Sulfide Films. I. Photoconduction. *Japanese Journal of Applied Physics* **1984**, *23*, 1614–1618.

(7) Mishra, R.; Sharma, A.; Tandon, P. Conducting Polymers — Modern Semiconductors : A Theoretical Overview.

(8) Barile, M.; Lecce, L.; Iannone, M.; Pappadà, S.; Roberti, P. In *Revolutionizing Aircraft Materials and Processes*; Pantelakis, S., Tserpes, K., Eds.; Springer International Publishing: Cham, 2020; pp 87–114, tex.ids= Barile:2020:RevolutionizingAircraftMaterialsandProcessesa.

(9) Ghanbari, L. N.; Crater, E. R.; Enos, N. R.; McNair, O. D.; Moore, R. B.; Wiggins, J. S. Polyphenylene sulfide for high-rate composite manufacturing: Impacts of processing parameters on chain architecture, rheology, and crystallinity. *Polymer Degradation and Stability* **2023**, *218*, 110580, tex.ids= Ghanbari:2023:PolymerDegradationandStability, Ghanbari:2023:PolymerDegradationandStabilitya.

(10) Uematsu, H.; Yoshida, K.; Yamaguchi, A.; Fukushima, A.; Sugihara, S.; Yamane, M.; Ozaki, Y.; Tanoue, S. Enhancement of interfacial shear strength due to cooperative - interaction between polyphenylene sulfide and carbon fiber and molecular orientation of polyphenylene sulfide via the - interaction. *Composites Part A: Applied Science and Manufacturing* **2023**, *165*, 107355.

(11) Mao, Z.; Li, T.; Zhan, H.; Wang, B. Molecular evolution mechanism of flow-induced

crystallization in polyphenylene sulfide. *International Journal of Mechanical Sciences* **2023**, *240*, 107917.

(12) Jiao, Y.; Ma, W. Effect of the polymer on the joint strength of polymer/copper hybrids produced by nano-injection molding: Comparison of polybutylene terephthalate and polyphenylene sulfide via experimental and computational methods. *Materials Today Communications* **2022**, *33*, 104291.

(13) Li, H.; Cai, Z.; Zhou, F.; Liu, D. MD simulation analysis of the anchoring behavior of injection-molded nanopits on polyphenylene sulfide/Cu interface. *Composite Interfaces* **2022**, *29*, 431–446.

(14) Yu, B.; Fu, S.; Wu, Z.; Bai, H.; Ning, N.; Fu, Q. Molecular dynamics simulations of orientation induced interfacial enhancement between single walled carbon nanotube and aromatic polymers chains. *Composites Part A: Applied Science and Manufacturing* **2015**, *73*, 155–165.

(15) Wang, X.; Zhao, T.; Zou, L.; Wang, X.; Zhang, L.; Yi, X. Molecular Dynamics Simulation of Pyrolysis and Electric-caused Disintegration Mechanism of Polyphenylene Sulfide. 2021 IEEE 4th International Electrical and Energy Conference (CIEEC). Wuhan, China, 2021; pp 1–6.

(16) Bishara, D.; Xie, Y.; Liu, W. K.; Li, S. A State-of-the-Art Review on Machine Learning-Based Multiscale Modeling, Simulation, Homogenization and Design of Materials. *Archives of Computational Methods in Engineering* **2023**, *30*, 191–222.

(17) Li, Y.; Abberton, B.; Kröger, M.; Liu, W. Challenges in Multiscale Modeling of Polymer Dynamics. *Polymers* **2013**, *5*, 751–832.

(18) Gooneie, A.; Schuschnigg, S.; Holzer, C. A Review of Multiscale Computational Methods in Polymeric Materials. *Polymers* **2017**, *9*, 16.

(19) Schmid, F. Understanding and Modeling Polymers: The Challenge of Multiple Scales. *ACS Polymers Au* **2023**, *3*, 28–58.

(20) Gartner, T. E.; Jayaraman, A. Modeling and Simulations of Polymers: A Roadmap. *Macromolecules* **2019**, *52*, 755–786.

(21) Dhamankar, S.; Webb, M. A. Chemically specific coarse-graining of polymers: Methods and prospects. *Journal of Polymer Science* **2021**, *59*, 2613–2643.

(22) Reith, D.; Meyer, H.; Müller-Plathe, F. Mapping atomistic to coarse-grained polymer models using automatic simplex optimization to fit structural properties. *Macromolecules* **2001**, *34*, 2335–2345.

(23) Reith, D.; Pütz, M.; Müller-Plathe, F. Deriving effective mesoscale potentials from atomistic simulations: Mesoscale Potentials from Atomistic Simulations. *Journal of Computational Chemistry* **2003**, *24*, 1624–1636.

(24) Moore, T. C.; Iacovella, C. R.; McCabe, C. Derivation of coarse-grained potentials via multistate iterative Boltzmann inversion. *The Journal of Chemical Physics* **2014**, *140*, 224104, tex.ids= Moore:2014:J.Chem.Phys.

(25) Izvekov, S.; Voth, G. A. Multiscale coarse graining of liquid-state systems. *The Journal of Chemical Physics* **2005**, *123*, 134105.

(26) Hynninen, A.-P.; Matthews, J. F.; Beckham, G. T.; Crowley, M. F.; Nimlos, M. R. Coarse-Grain Model for Glucose, Cellobiose, and Cellotetraose in Water. *Journal of Chemical Theory and Computation* **2011**, *7*, 2137–2150.

(27) Shell, M. S. The relative entropy is fundamental to multiscale and inverse thermodynamic problems. *The Journal of Chemical Physics* **2008**, *129*, 144108.

(28) Shell, M. S. Systematic coarse-graining of potential energy landscapes and dynamics in liquids. *The Journal of Chemical Physics* **2012**, *137*, 084503.

(29) Zhang, X.-Z.; Lu, Z.-Y.; Qian, H.-J. Temperature Transferable and Thermodynamically Consistent Coarse-Grained Model for Binary Polymer Systems. *Macromolecules* **2023**, *56*, 3739–3753.

(30) Bayramoglu, B.; Faller, R. Modeling of Polystyrene under Confinement: Exploring the Limits of Iterative Boltzmann Inversion. *Macromolecules* **2013**, *46*, 7957–7976.

(31) Choudhury, C. K.; Carbone, P.; Roy, S. Scalability of Coarse-Grained Potentials Generated from Iterative Boltzmann Inversion for Polymers: Case Study on Polycarbonates. *Macromolecular Theory and Simulations* **2016**, *25*, 274–286, tex.ids= choudhuryScalabilityCoarseGrainedPotentials2016a.

(32) Harmandaris, V. A.; Adhikari, N. P.; Van Der Vegt, N. F. A.; Kremer, K. Hierarchical Modeling of Polystyrene: From Atomistic to Coarse-Grained Simulations. *Macromolecules* **2006**, *39*, 6708–6719.

(33) Moore, T. C.; Iacovella, C. R.; Hartkamp, R.; Bunge, A. L.; McCabe, C. A Coarse-Grained Model of Stratum Corneum Lipids: Free Fatty Acids and Ceramide NS. *Journal of Physical Chemistry B* **2016**, *120*, 9944–9958.

(34) Moore, T. C.; Iacovella, C. R.; Leonhard, A. C.; Bunge, A. L.; McCabe, C. Molecular dynamics simulations of stratum corneum lipid mixtures: A multiscale perspective. *Biochemical and Biophysical Research Communications* **2018**, *498*, 313–318, Publisher: Elsevier Ltd.

(35) Tang, J.; Kobayashi, T.; Zhang, H.; Fukuzawa, K.; Itoh, S. Enhancing pressure consistency and transferability of structure-based coarse-graining. *Physical Chemistry Chemical Physics* **2023**, *25*, 2256–2264.

(36) Wang, K. W.; Wang, Y.; Hall, C. K. Development of a coarse-grained lipid model, LIME 2.0, for DSPE using multistate iterative Boltzmann inversion and discontinuous molecular dynamics simulations. *Fluid Phase Equilibria* **2020**, *521*, 112704.

(37) Albooyeh, M.; Jones, C.; Barrett, R.; Jankowski, E. FlowerMD: Flexible Library of Organic Workflows andExtensible Recipes for Molecular Dynamics. *Journal of Open Source Software* **2023**, *8*, 5989.

(38) Anderson, J. A.; Glaser, J.; Glotzer, S. C. HOOMD-blue: A Python package for high-performance molecular dynamics and hard particle Monte Carlo simulations. *Computational Materials Science* **2020**, *173*, 109363, tex.ids= Anderson:2020:ComputationalMaterialsScience, andersonHOOMDbluePythonPackage2020.

(39) Adorf, C. S.; Dodd, P. M.; Ramasubramani, V.; Glotzer, S. C. Simple data and workflow management with the signac framework. *Computational Materials Science* **2018**, *146*, 220–229, tex.ids= Adorf:2018:ComputationalMaterialsScience.

(40) Lennard-Jones, J. The electronic structure of some diatomic molecules. *Transactions of the Faraday Society* **1929**, *25*, 668–686.

(41) Jorgensen, W. L.; Tirado-Rives, J. The OPLS [optimized potentials for liquid simulations] potential functions for proteins, energy minimizations for crystals of cyclic peptides and crambin. *Journal of the American Chemical Society* **1988**, *110*, 1657–1666.

(42) Klein, C.; Summers, A. Z.; Thompson, M. W.; Gilmer, J. B.; McCabe, C.; Cummings, P. T.; Sallai, J.; Iacovella, C. R. Formalizing atom-typing and the dissemination of force fields with foyer. *Computational Materials Science* **2019**, *167*, 215–227, tex.ids= Klein:2019:ComputationalMaterialsScience.

(43) Chodera, J. D.; Swope, W. C.; Pitera, J. W.; Seok, C.; Dill, K. A. Use of the Weighted Histogram Analysis Method for the Analysis of Simulated and Parallel Tempering Simulations. *Journal of Chemical Theory and Computation* **2007**, *3*, 26–41.

(44) Shirts, M. R.; Chodera, J. D. Statistically optimal analysis of samples from multiple equilibrium states. *The Journal of Chemical Physics* **2008**, *129*, 124105.

(45) Roe, R.-J. In *Atomistic Modeling of Physical Properties*; Monnerie, L., Suter, U. W., Eds.; Springer Berlin Heidelberg, 1994; Vol. 116; pp 111–144, Series Title: Advances in Polymer Science.

(46) Patrone, P. N.; Dienstfrey, A.; Browning, A. R.; Tucker, S.; Christensen, S. Uncertainty quantification in molecular dynamics studies of the glass transition temperature. *Polymer* **2016**, *87*, 246–259.

(47) Bulacu, M.; van der Giessen, E. Molecular-dynamics simulation study of the glass transition in amorphous polymers with controlled chain stiffness. *Physical Review E* **2007**, *76*, 011807, tex.ids= Bulacu:2007:Phys.Rev.E.

(48) Henry, M. M.; Thomas, S.; Alberts, M.; Estridge, C. E.; Farmer, B.; McNair, O.; Jankowski, E. General-Purpose Coarse-Grained Toughened Thermoset Model for 44DDS/DGEBA/PES. *Polymers* **2020**, *12*, 2547.

(49) Kalkar, A.; Deshpande, V.; Kulkarni, M. Isothermal crystallization kinetics of poly(phenylene sulfide)/TLCP composites. *Polymer Engineering & Science* **2009**, *49*, 397–417.

(50) Ramasubramani, V.; Dice, B. D.; Harper, E. S.; Spellings, M. P.; Anderson, J. A.; Glotzer, S. C. freud: A software suite for high throughput analysis of particle simulation data. *Computer Physics Communications* **2020**, *254*, 107275.

(51) Gowers, R.; Linke, M.; Barnoud, J.; Reddy, T.; Melo, M.; Seyler, S.; Domański, J.; Dotson, D.; Buchoux, S.; Kenney, I.; Beckstein, O. MDAnalysis: A Python Package for the Rapid Analysis of Molecular Dynamics Simulations. Austin, Texas, 2016; pp 98–105.

(52) Michaud-Agrawal, N.; Denning, E. J.; Woolf, T. B.; Beckstein, O. MDAnalysis: A toolkit for the analysis of molecular dynamics simulations. *Journal of Computational Chemistry* **2011**, *32*, 2319–2327.

(53) Tabor, B. J.; Magré, E. P.; Boon, J. The crystal structure of poly-p-phenylene sulphide. *European Polymer Journal* **1971**, *7*, 1127–1133, tex.ids= Tabor:1971:Eur.Polym.J.

(54) Lovinger, A. J.; Padden, F. J.; Davis, D. D. Structure of poly(p-phenylene sulphide). *Polymer* **1988**, *29*, 229–232.

(55) Sigaud, G.; Yoon, D. Y.; Griffin, A. C. Order in nematic phase of semiflexible polymers. *Macromolecules* **1983**, *16*, 875–880.

(56) Hu, W.; Frenkel, D. In *Interphases and Mesophases in Polymer Crystallization III*; Allegra, G., Ed.; Springer-Verlag: Berlin/Heidelberg, 2005; Vol. 191; pp 1–35, Series Title: Advances in Polymer Science.

(57) Lu, S. X.; Cebe, P. Effects of annealing on relaxation behavior and charge trapping in film-processed poly(phenylene sulfide). *Journal of Applied Polymer Science* **1996**, *61*, 473–483, tex.ids= luEffectsAnnealingRelaxation1996.

(58) Vettorel, T.; Meyer, H. Coarse graining of short polythylene chains for studying polymer crystallization. *Journal of Chemical Theory and Computation* **2006**, *2*, 616–629.

(59) Marsh, H. S.; Jankowski, E.; Jayaraman, A. Controlling the Morphology of Model Conjugated Thiophene Oligomers through Alkyl Side Chain Length, Placement, and Interactions. *Macromolecules* **2014**, *47*, 2736–2747.

(60) Jones, M. L.; Jankowski, E. Computationally connecting organic photovoltaic performance to atomistic arrangements and bulk morphology. *Molecular Simulation* **2017**, *43*, 756–773, Publisher: Taylor & Francis.

(61) Greco, C.; Melnyk, A.; Kremer, K.; Andrienko, D.; Daoulas, K. C. Generic Model for Lamellar Self-Assembly in Conjugated Polymers: Linking Mesoscopic Morphology and Charge Transport in P3HT. *Macromolecules* **2019**, *52*, 968–981.

(62) Meyer, H.; Müller-Plathe, F. Formation of chain-folded structures in supercooled polymer melts. *The Journal of Chemical Physics* **2001**, *115*, 7807–7810.

(63) Gay, J. G.; Berne, B. J. Modification of the overlap potential to mimic a linear site-site potential. *The Journal of Chemical Physics* **1981**, *74*, 3316–3319.

(64) Becerra, D.; Jois, P. R.; Hall, L. M. Coarse-grained modeling of polymers with end-on and side-on liquid crystal moieties: effect of architecture. *The Journal of Chemical Physics* **2023**, *158*, 224901, arXiv:2212.09978 [cond-mat].

(65) Walsh, T. R. Towards an anisotropic bead-spring model for polymers: a Gay-Berne parametrization for benzene. *Molecular Physics* **2002**, *100*, 2867–2876.

(66) Chen, W.; Zhu, Y.; Cui, F.; Liu, L.; Sun, Z.; Chen, J.; Li, Y. GPU-Accelerated Molecular Dynamics Simulation to Study Liquid Crystal Phase Transition Using Coarse-Grained Gay-Berne Anisotropic Potential. *PLOS ONE* **2016**, *11*, e0151704.

(67) Cohen, A. E.; Jackson, N. E.; Pablo, J. J. D. Anisotropic Coarse-Grained Model for Conjugated Polymers: Investigations into Solution Morphologies. *Macromolecules* **2021**, *54*, 3780–3789.

(68) Nguyen, H. T. L.; Huang, D. M. Systematic bottom-up molecular coarse-graining via force and torque matching using anisotropic particles. *Journal of Chemical Physics* **2022**, *156*, tex.ids= nguyenSystematicBottomupMolecular2022a publisher: AIP Publishing, LLC.

(69) Jin, J.; Pak, A. J.; Durumeric, A. E. P.; Loose, T. D.; Voth, G. A. Bottom-up Coarse-Graining: Principles and Perspectives. *Journal of Chemical Theory and Computation* **2022**, *18*, 5759–5791.

(70) Wang, J.; Olsson, S.; Wehmeyer, C.; Pérez, A.; Charron, N. E.; De Fabritiis, G.; Noé, F.;

Clementi, C. Machine Learning of Coarse-Grained Molecular Dynamics Force Fields. *ACS Central Science* **2019**, *5*, 755–767, tex.ids= Wang:2019:ACSCent.Sci.a.

(71) Joshi, S. Y.; Deshmukh, S. A. A review of advancements in coarse-grained molecular dynamics simulations. *Molecular Simulation* **2021**, *47*, 786–803.

(72) Ricci, E.; Vergadou, N. Integrating Machine Learning in the Coarse-Grained Molecular Simulation of Polymers. *The Journal of Physical Chemistry B* **2023**, *127*, 2302–2322.

(73) Wilson, M. O.; Huang, D. M. Anisotropic molecular coarse-graining by force and torque matching with neural networks. *The Journal of Chemical Physics* **2023**, *159*, 024110.

(74) Singraber, A.; Behler, J.; Dellago, C. Library-Based *LAMMPS* Implementation of High-Dimensional Neural Network Potentials. *Journal of Chemical Theory and Computation* **2019**, *15*, 1827–1840.

(75) Duignan, T. T. The Potential of Neural Network Potentials. *ACS Physical Chemistry Au* **2024**, *4*, 232–241.